

# **Exploration of Utilizing Bernoulli's Principle to Monitor Oxygen Flow in Split Ventilator Lines**

**Gavin DeBrun, Daniel Foster, Nicholas Piunti**

## **Abstract**

In this paper, we discuss our investigation of the properties of an insertable oxygen flow rate monitor for use in split ventilator lines. Due to the COVID-19 pandemic, healthcare professionals are facing the challenge of intubating patients beyond existing ventilator availability. As a result, healthcare workers are forced to either split ventilator lines, or to make the difficult decision not to intubate patients that otherwise would be (Rosenthal, 2020). In our attempt to design an accurate, unobstructive insertable device to monitor oxygen flow using inexpensive materials, we leveraged the Bernoulli principle to monitor the flow rate by calculating pressure differences between sections of an insertable tube that had differing cross sectional areas. We found that, at flow rates of 0.5 liters per second and 1 liter per second (the typical range of inspiratory flow rate (Warner and Patel, 2013)), our device achieved accuracies of  $86 \pm 12\%$  and at least 93% respectively. Further exploration is necessary; however, our results are promising, and the resulting product may help address the ongoing ventilator shortage, especially in developing nations that have minimal ventilator supply.

## **Background**

Mechanical ventilation has been around for many decades as a method to provide oxygen and remove carbon dioxide for patients who are unable to do so themselves. In more developed countries, the need for ventilation is generally met by the healthcare system. In less developed

countries, it can be difficult or impossible to find a ventilator in their hospitals. According to Maclean and Marks (2020), there are ten countries in Africa that do not have any ventilators in their hospitals. The ones that do have ventilators are in a similar situation to South Sudan, a country of 11 million with a total of four ventilators. Hospitals in more developed nations may be able to keep up with the demand for ventilators during regular operations, but the COVID-19 pandemic has put a strain on many of their resources. The United States has 20.5 ICU beds with ventilator capacity per 100,000 residents (Hurtado, 2018). A study in *Crit Care Med* (2020) revealed that during the peak of the pandemic, 3-5% of cases required intensive care. Such strain on the healthcare system has resulted in doctors splitting ventilators among patients, in an attempt to provide care to more people at the same time. This measure has received emergency approval from the US FDA (2021). One of the suggested guidelines is the inclusion of flow/pressure monitors to ensure that the oxygen intake needs of the patients are met. In this project, we sought a cheap and reliable method to measure the volume of air being delivered to intubated patients that can be easily implemented in the healthcare setting.

Pressure sensors added to the ventilator tubes can be used to monitor the rate of oxygen flow. By attaching a tube insert with a constriction in the middle and comparing pressure readings between the non-constricted input section and the constriction section, one can calculate the rate at which oxygen is pumped out of the ventilator.

We considered a variety of methods in order to determine the optimal procedure to measure airflow. Some of the important metrics considered include cost, ease of use, accuracy, manufacturing time, and flow obstruction. We concluded that we wanted to find an insert that can be connected to the ventilation lines and measure the flow rate digitally. This would make it easy to use and maintain. We decided to measure the flow of air using pressure sensors by

making use of Bernoulli's Principle. This principle is only valid for an incompressible flow; however, below velocities of Mach 0.3, compressible fluids such as oxygen are accurately described using Bernoulli's equation (Anderson, 2007). As the flow velocities of ventilation are orders of magnitude lower than this value, such an approximation is suitable. The internal energy of a fluid can be expressed in terms of the pressure and velocity of flow. As a result, by increasing the velocity of the fluid, a decrease in pressure can be measured at a given location. This change in pressure and velocity is dependent on the initial velocity of the fluid. Measuring the change in the pressure of a gas, via this relation, allows for measurement of its velocity. In order to make use of this effect, we decided that our designs would incorporate a tube with a narrow section to change the speed of the airflow. Pressure sensors would then be placed at each end and in the center constriction. Fortunately, there are accurate digital pressure sensors with a high resolution available at a low cost. The pressure sensors can then be run through a microcontroller, which supplies power to the sensors, controls the measurements, and interprets measured data. This affords us a degree of flexibility in data collection and analysis. Additionally, a 3D printer allows us to quickly and easily make changes to the design of the tube, as the design was optimized.

### Methods/Procedures

We decided to use Bernoulli's Principle to convert our pressure readings to a flow rate. Bernoulli's Principle uses the conservation of energy to relate the pressure and speed of a fluid within a known cross-sectional area. We begin deriving the equation by finding the total energy in a given cross-section of flow. Three types of energy are seen here: energy from the pressure, as well as kinetic and potential energy:

$$E_{tot} = PV + \frac{1}{2}mv^2 + mgh \quad (1)$$

By summing together the energies in each section of flow and dividing by the volume of air, we receive the following equation:

$$P_1 + \frac{1}{2}\rho v_1^2 + \rho gh_1 = P_2 + \frac{1}{2}\rho v_2^2 + \rho gh_2 \quad (2)$$

Since the tube is level, we can remove the potential energy terms:

$$P_1 + \frac{1}{2}\rho v_1^2 = P_2 + \frac{1}{2}\rho v_2^2 \quad (3)$$

We can relate the flow velocity  $v$  to a volume flow rate  $Q$  by multiplying by the cross-sectional area. Thus:

$$P_1 + \frac{1}{2}\rho\left(\frac{Q}{A_1}\right)^2 = P_2 + \frac{1}{2}\rho\left(\frac{Q}{A_2}\right)^2 \quad (4)$$

Solving for  $Q$  (in cubic meters per second) gives

$$Q = \sqrt{\frac{2\Delta P}{\rho} \frac{1}{\frac{1}{A_2^2} - \frac{1}{A_1^2}}} \quad (5)$$

We now have our equation that will relate our sensor readings to a calculable flow rate.

The pressure sensor used was Adafruit's DPS310 Precision Barometric Pressure / Altitude Sensor. According to the data sheet from Infineon (2020), it can read pressures between 300 and 1200 hPa, with a precision of  $\pm 0.2$  Pa (or a 0.02 meter change in elevation), a relative accuracy of  $\pm 6$  Pa (0.5 m), and an absolute accuracy of  $\pm 100$  Pa (or 8 m). We tested the accuracy of the sensor by measuring the average of 100 pressure readings at a certain elevation and repeating for 4, 8, 12, 16, and 20 cm above that baseline elevation. The results can be seen in

Figure 1. The slope here is almost 0.1 hPa/m, which roughly matches the precision stated on the datasheet.

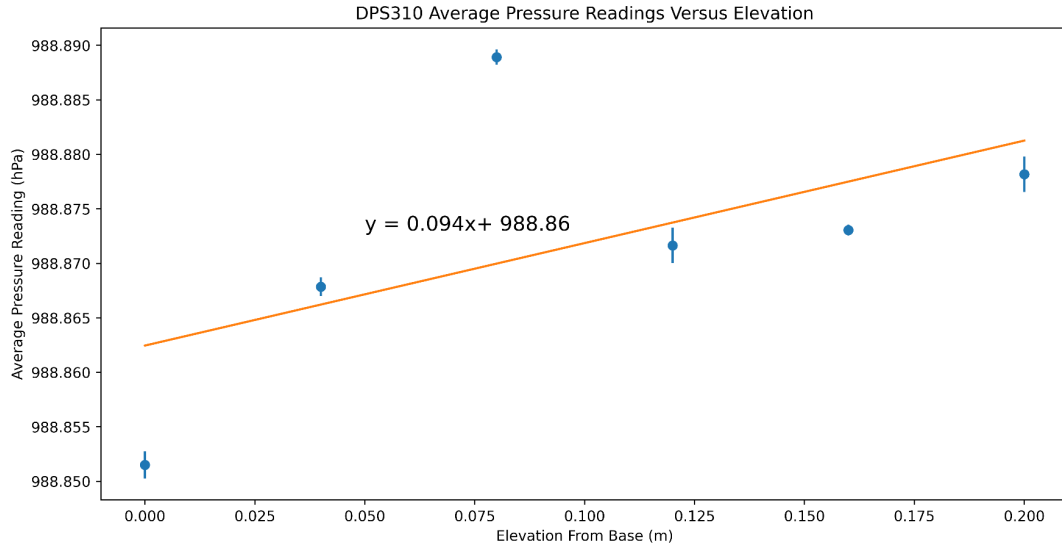


Figure 1. Elevation vs. pressure plot for a DPS310 unit. Means are plotted with error bars representing the spread of the data.

Four DPS310s are used for each insert - one on the input and on the output, one in the constriction, and one outside the tube to be used as a control. These sensors were wired using I2C to an Adafruit Feather M0 with long-range radio capabilities. Since the DPS310s all share an I2C address, we had to connect them via a TCA9548A I2C multiplexer. We also connected a real-time clock using I2C and used an Adafruit GPS breakout module to set the time. This would allow us to place timestamps on our readings. We also attached a microSD breakout using SPI to save our readings, and an LCD screen so system messages could be delivered to the user without requiring connection to a computer. The circuit schematic as well as the finalized circuit board are shown in Figure 2. We instructed the microcontroller to send flow monitoring data via radio

to an external base station, so that patients could be monitored without having to be present. This allows for one person to receive data from several inserts and read them all at one location.

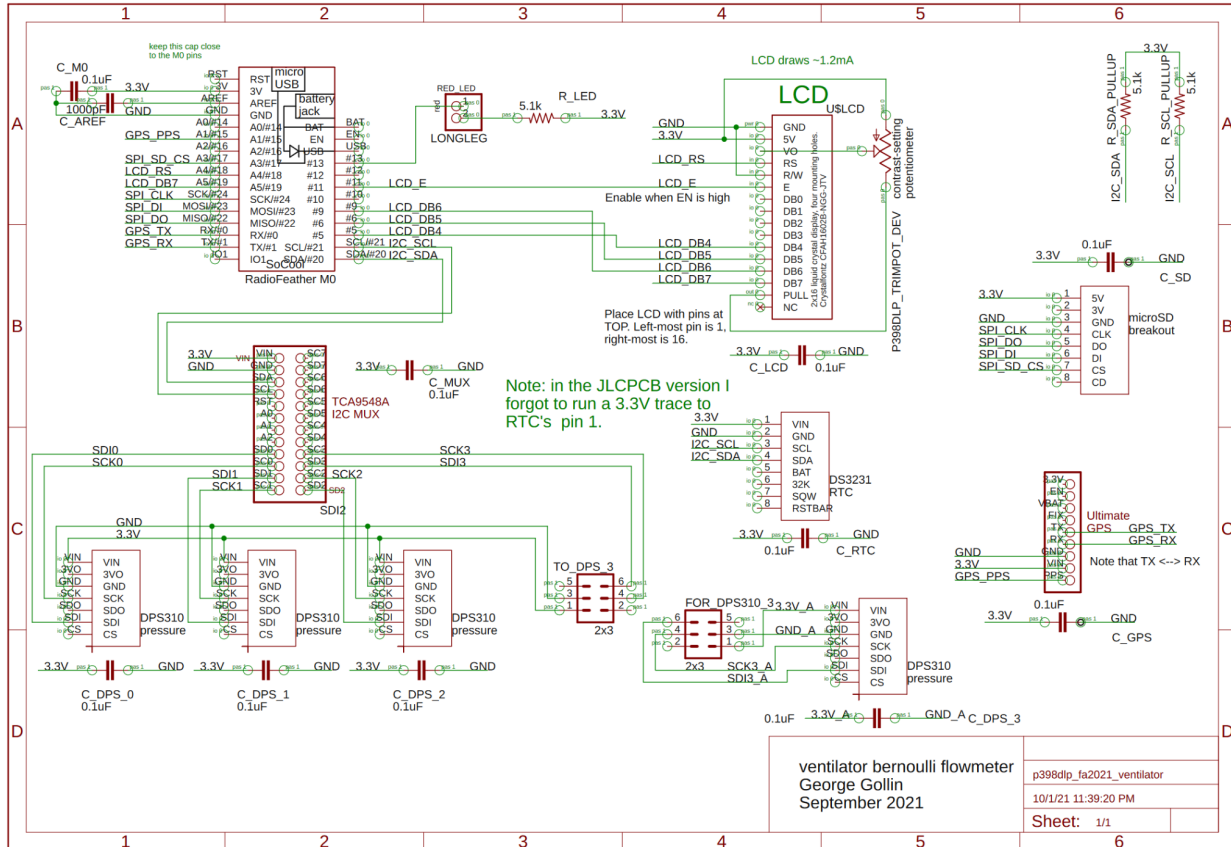


Figure 2. Top: circuit schematic for the ventilator tube insert. Bottom: printed circuit board.

We decided to make a rectangular tube with larger ends and a constriction in the middle.

We left holes in the bottom so we could access the pins on the DPS310 pressure sensors, as shown in Figure 3. The insert is 2 cm wide. The ends are 2.5 cm tall, while the constriction in the

center is 0.5 cm tall. (The completed design, including the circuit board, is shown in Figure 5.)

By using the insert's cross-sectional areas in Equation 5, and assuming air at 20°C ( $\rho = 1.21$  kg/m<sup>3</sup>) we determined that the pressure difference should be 58.08 Pa for a flow rate of one L/s, which is the inspiratory flow rate used by most ventilators (Alex).

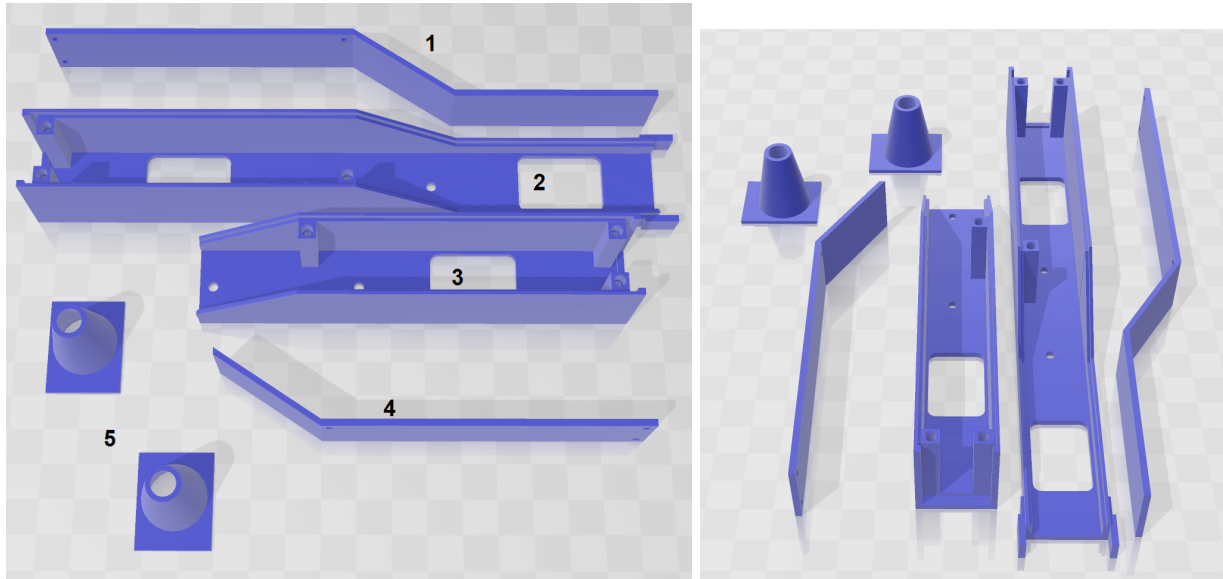


Figure 3. The disassembled insert. Pictured: (1) first half of lid, (2) first half of tube, (3) second half of tube, (4) second half of lid, (5) nozzles for attaching vinyl tubing. Rectangular holes in the tube serve as locations for the DPS310 units. Each grid square is 10 mm on a side.

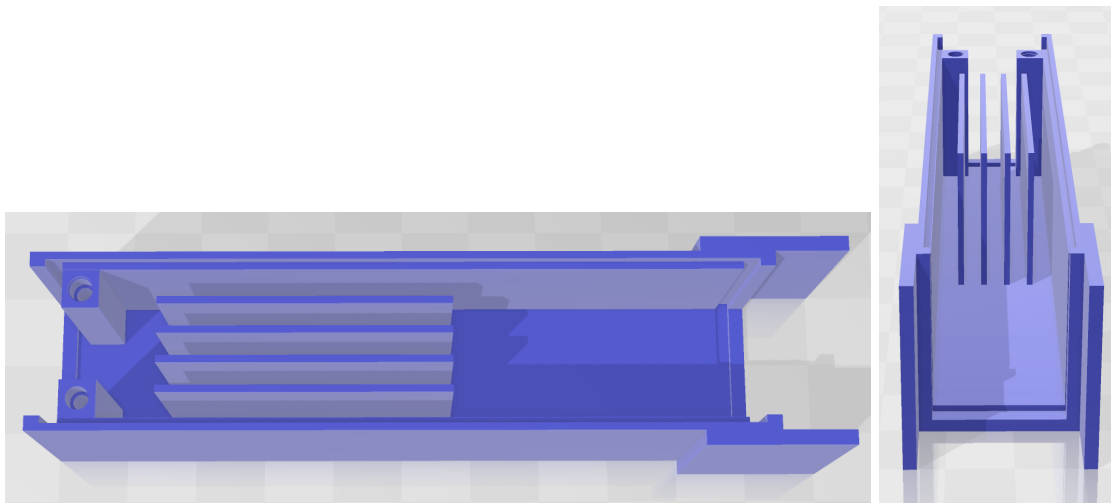


Figure 4. Top and front views of the diffuser, used in later parts of testing.

In order to begin data collection, we attached an air mattress pump and a PRM FMDFG03 airflow meter in series with a ball valve and the device as shown in Figure 6. Connections were made using vinyl tubing, hose clamps, and duct tape. Our data collection focused on measuring the pressures of all four DPS310 sensors over varying input volume flow rates. We programmed a data acquisition program in Arduino C++ and uploaded it to the Feather M0 microcontroller via the Arduino IDE for each experimental trial. The data was saved to a microSD card for offline analysis. The Arduino IDE's serial monitor was used to initialize trials and label data points based on relevant parameters such as the expected flow rate which was measured on the PRM flow meter and adjusted with the ball valve. At the beginning of a trial, the ambient atmospheric pressure sensor and all three internal pressure sensors recorded a set number of readings every 200 ms with the pump off and no flow passing through the tube. After this ambient calibration reading, the averages of the readings for each sensor were calculated and stored to offset later pump-on readings. After turning on the pump and using the external volume flow meter to reach a given flow rate, we took a set number of pressure readings. The actual pressure increase for each sensor was calculated by averaging its pump-on measurements and then subtracting the average of its pump-off measurements. This was done to account for manufacturing differences of the individual DPS310s and it allowed us to calculate the true pressure differences between sensors. To further examine pressure increases due to the airflow, we calculated the change in pressure of the ambient pressure sensor between the pump-off measurements and pump-on measurements in the same way. We then subtracted this value from the calculated pressure increases for each internal sensor to adjust for changes in atmospheric pressure. As each offset between any given pair of pressure sensors was assumed to be constant,

we calculated the actual pressure difference due to airflow between any pair of sensors by subtracting the pressure increase of one sensor from another. The input flow rate was changed by adjusting the ball valve until the PRM flow meter displayed the desired expectation value. We incremented the flow rate by each tick mark on the PRM flow meter, which corresponded to a change of 0.047 L/s. For each incremental input flow rate, we ran multiple trials with varying numbers of samples. Using the calculated pressure increases, the data acquisition program, using Equation 5, calculated, stored, and transmitted the measured input flow rate. As predicted by Bernoulli's equation, we sought a linear relationship between the measured pressure difference and the square of the input flow rate.



Figure 5. The initial design used for testing, with the diffuser attached on the input side. Labels: LCD (1), DS3231 real-time clock (2), microSD breakout (3), GPS (4), I2C multiplexer (5), radio microcontroller (6), diffuser (7), constriction (8), output end (9).



Figure 6. Experimental setup consisting of main insert (1), extended insert (2), vinyl tubing (3), PRM FMDFG03 airflow meter (4), air pump (5).

We considered turbulence as a potential source of error, so we tested the effect of a diffuser (shown in Figure 4) on the input in reducing turbulent flow. We also created an insert with an extended middle section as shown in Figures 7-8, to measure the effects of loss within the insert. Furthermore, we compared using the system with the diffuser on the input versus the output and tested a tube with some amount of leakage.

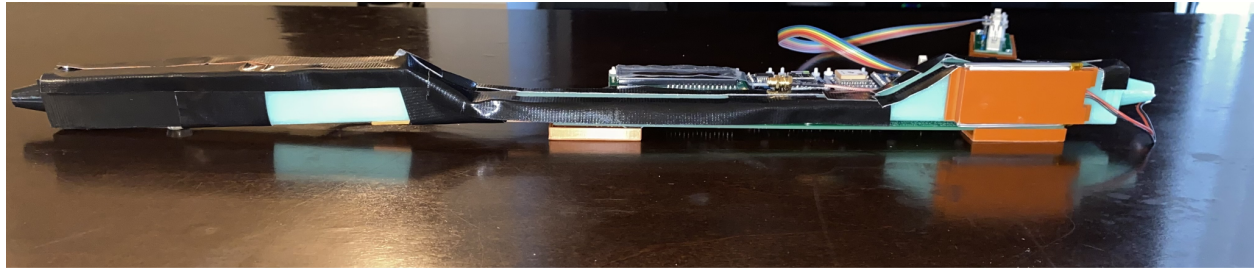


Figure 7. Side view of the extended insert.

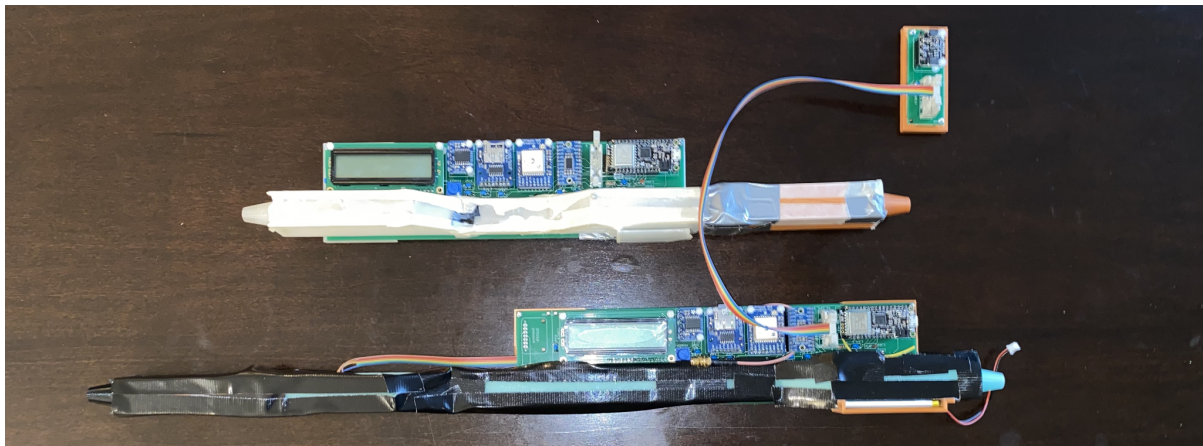


Figure 8. Comparison of the initial and extended inserts.

## Results

For the version of the tube with a diffuser on the input, we measured the pressure difference between the input sensor and the constriction sensor across a range of flow rates; Figure 9 was produced as a calibration curve. From Figure 9, you can see a strong linear fit, as a result of the high r-square value. Additionally, there is a sharp tail around the start of the curve and the slope decreases slightly with higher values.

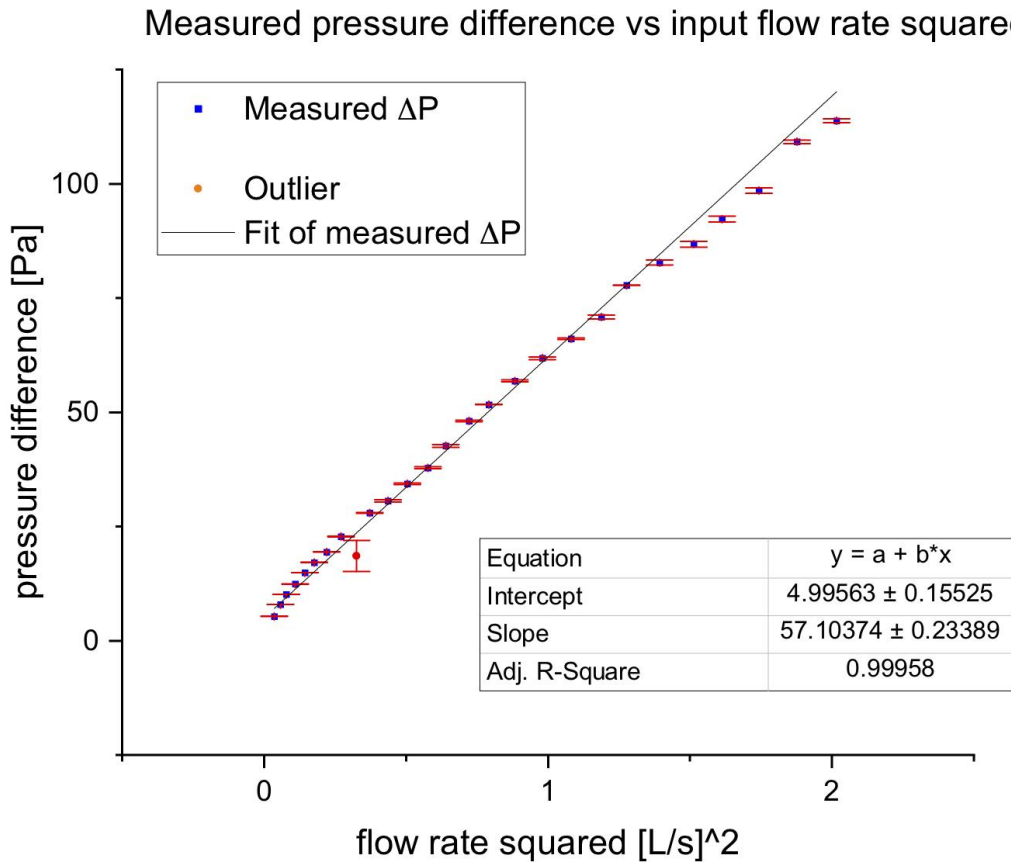


Figure 9: The calibration curve for the tube with a diffuser on the input. The error of each point is calculated using the standard deviation.

Converting the pressure differences seen in Figure 9 into flow rates using Equation 5 and subtracting the expected flow rate as measured by the PRM external flow meter, we observe that at lower expected input flow rates there is a higher difference between the measured flow rate and the expected flow rate. This downward trend continues until an input flow rate of approximately 1.1 L/s at which our measured flow rates drop below the expected flow rate. This

relationship is exhibited in Figure 10. Furthermore, we see that our residuals appear to be randomly distributed, indicating that a linear fit is an accurate model.

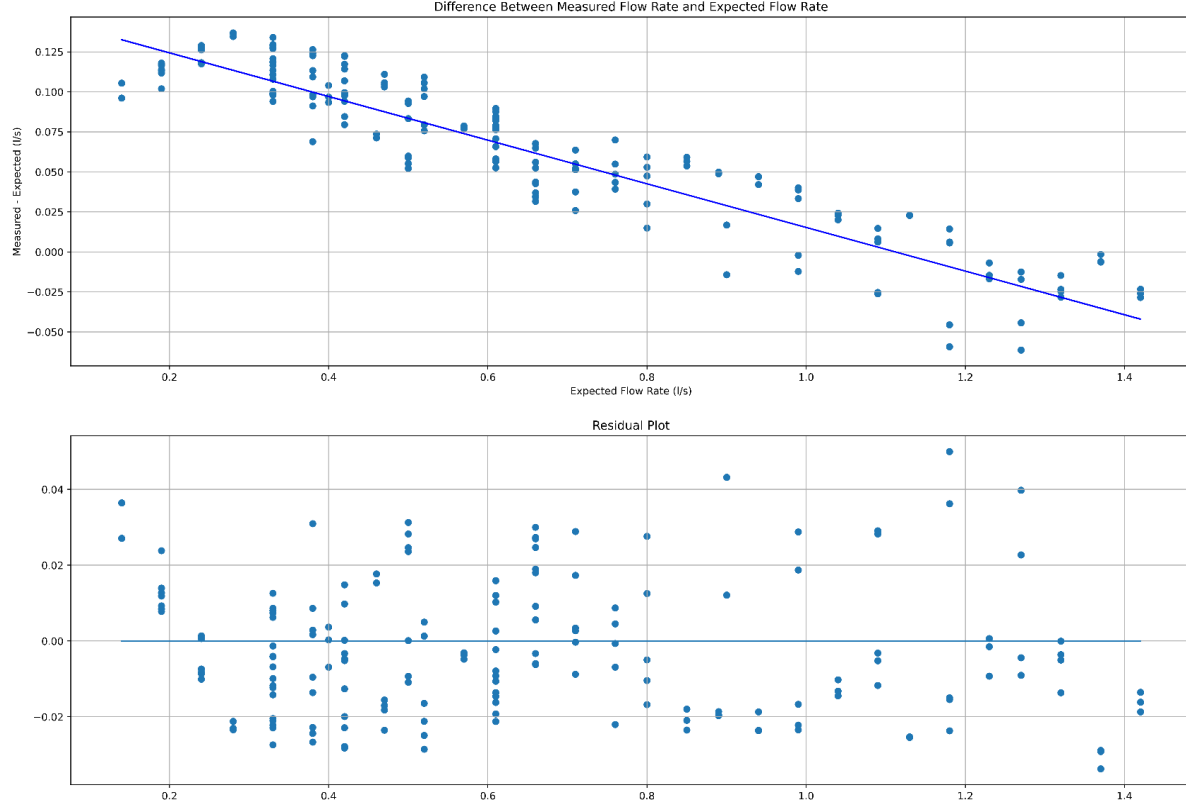


Figure 10: The difference between the flow rate measured by our device and the expected input flow rate as measured by the external air flow meter. Fewer data points were collected at higher expected flow rates.

Averaging the measured flow rates for each unique expected input flow rate (as we ran multiple trials at each input flow rate) allows us to more clearly observe the relationship demonstrated by Figure 10. Figure 11 shows the difference between the average measured flow rate and the expected flow rate for each expected input flow rate as well as the error. The error for the average measured flow rate is a result of variance in the individual measurements for each

unique input flow rate. The average standard deviation of the measured flow rates across the range of input flow rates is approximately 0.009 L/s. The standard deviation for the expected flow rate is a result of limitations of the PRM external flow meter and is a constant value of .057 L/s. Again, our residuals appear to be randomly distributed.

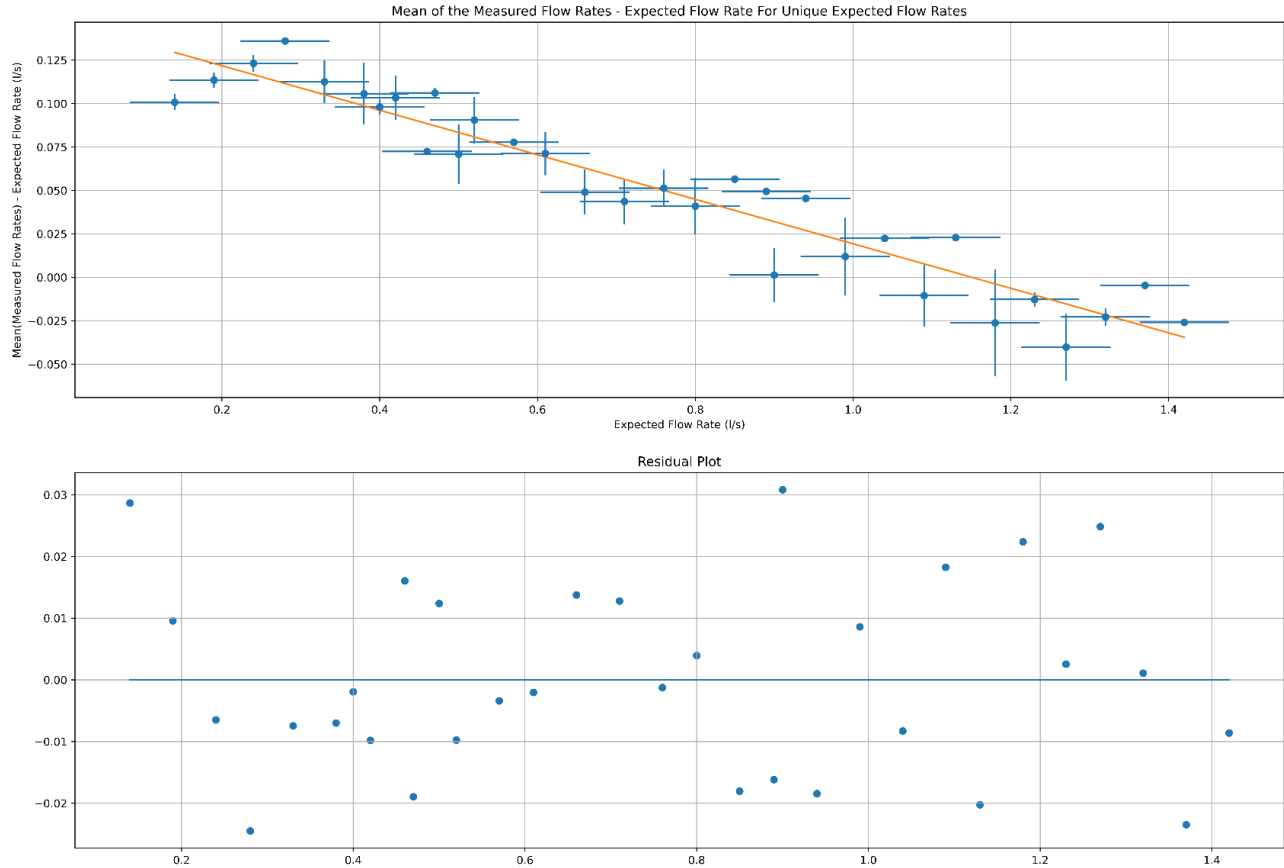


Figure 11: The difference between the average of the measured flow rates and the expected input flow rate for each expected input flow rate.

To examine the effect of the diffuser on measured flow rates, we can separate the data that was collected with the diffuser on the input from the data that was collected with the diffuser on the output. The results can be seen in Figures 12A and 12B. We observe the same downward trend, however observe that the orientation with the diffuser on the output (effectively no

diffuser), over the range of 0.5 L/s to 1 L/s, has smaller differences between the measured flow rates and the expected flow rates than the orientation with the diffuser on the input. The errors seen in figure 12B are caused by the same factors discussed previously. The average standard deviation across the range of input flow rates for the diffuser on input orientation is approximately .005 L/s while the average standard deviation across the range of input flow rates for the diffuser on output orientation is approximately .006 L/s. Furthermore, the residuals do not appear to be normally distributed, indicating that the data do not follow a simple linear fit and that a different model may be more accurate.

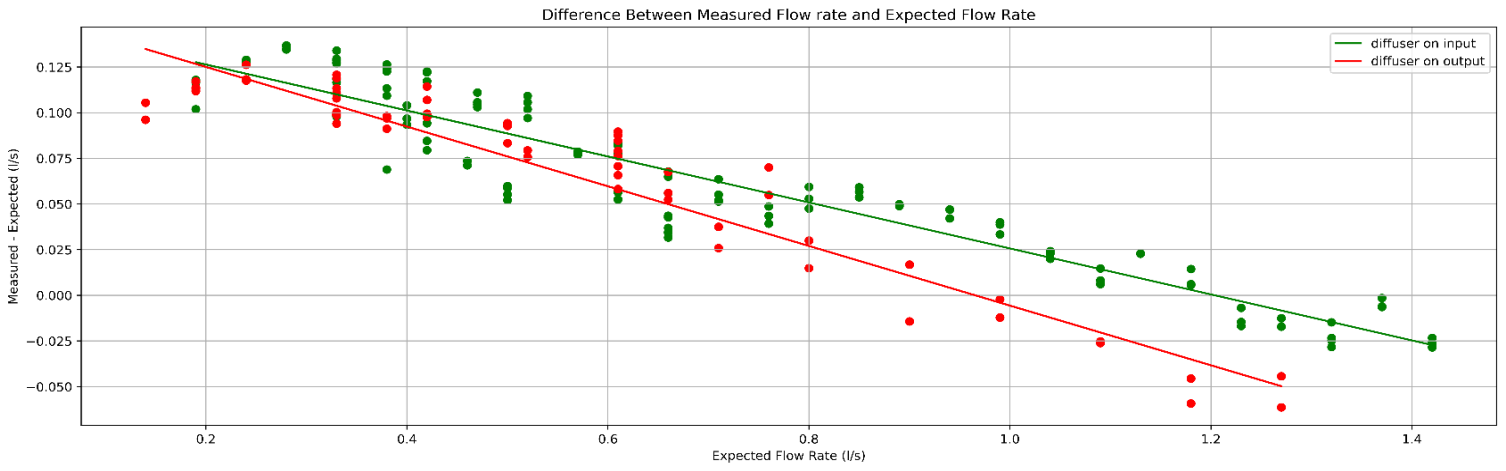


Figure 12A: Difference between the measured flow rate and the expected input flow rate for the diffuser on the input and the diffuser on the output.

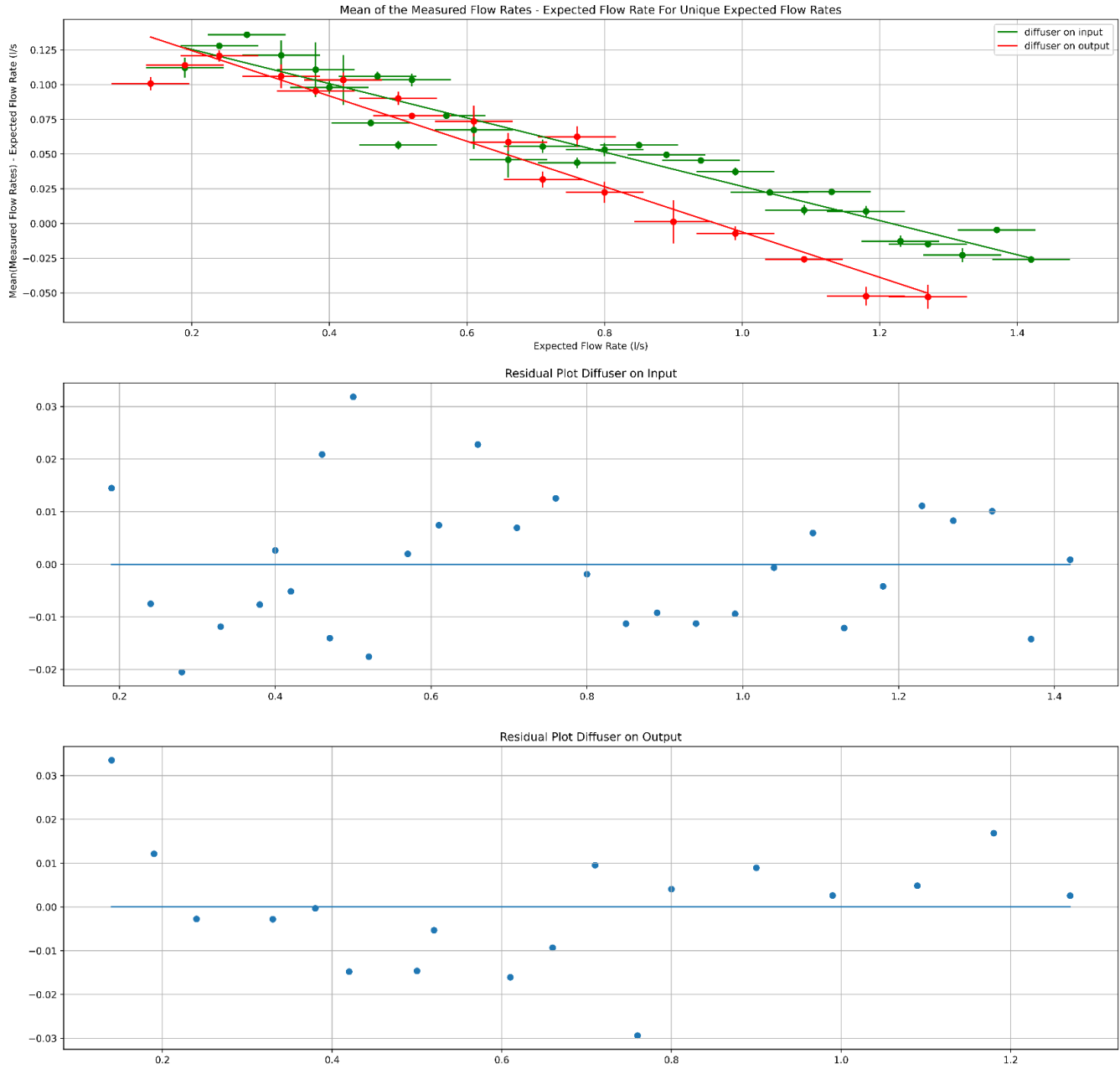


Figure 12B: The difference between the average of the measured flow rates and the expected input flow rate for each expected input flow rate for the diffuser on the input and output.

The final, elongated version of the tube had obvious leakage as evidenced by air being felt around the tube as the pump was on. In order to quantify this, data were collected by measuring the flow pressure differences across a range of flow rates. First, this was completed

with the tube as is, and then the leaks were sealed with glue and tape before the other measurements were made. Figure 13 shows the two data sets comparing the recorded pressure difference and the square of the input flow rate.

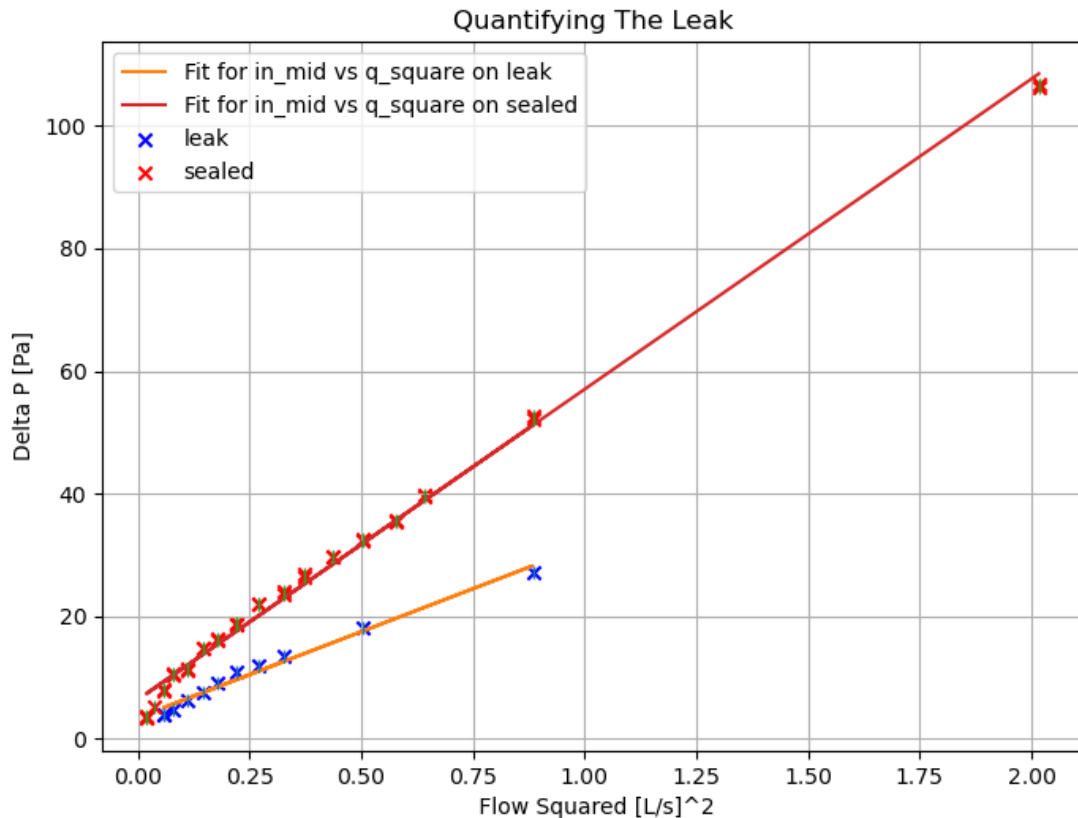


Figure 13: A plot comparing the square of the flow rate to its associated pressure difference between the input and constriction sensors. Note the difference between the fits of the data sets with leakage and without leakage.

A linear fit of the data with leakage reveals a slope of 28.030, and an intercept of 3.4596. A linear fit performed on the sealed tube reveals a slope of 50.64, and an intercept of 6.41. By substituting the density of air and the two cross sectional areas of the tube into Bernoulli's

equation and multiplying by the square of the conversion factor between cubic meters per second to liters per second, we see that the expected slope is 58.08. Additionally, there should be no intercept value predicted by the equation. Evidently, the slope of the sealed tube is larger than the one with leakage. Additionally, both plots show the linear trend breaks down for low flow rates, with this tail sharper for the sealed tube.

### Discussion

One of the first concerns with our setup was the effect that turbulence could potentially have on the pressure readings. Turbulence occurs in a fluid when the flow becomes unstable and the layers of the fluid do not travel parallel to each other. This introduces phenomena such as vortices where different parts of the fluid swirl and mix in an unpredictable fashion. This behavior is illustrated in Figure 14 (Nuclear Power).

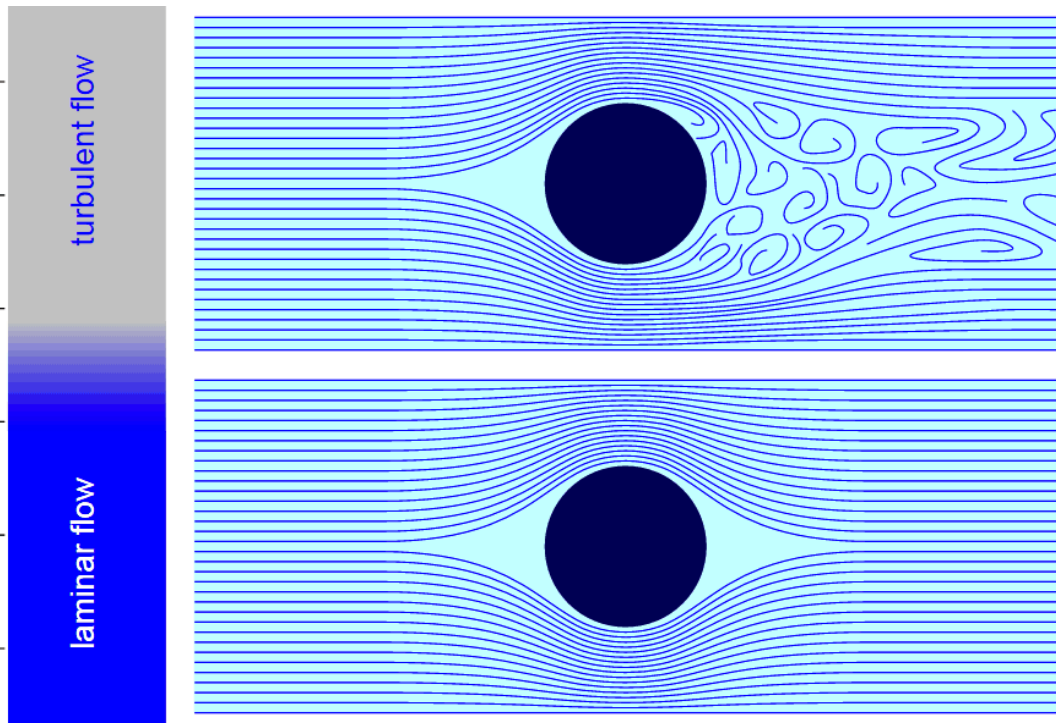


Figure 14: An illustration comparing turbulent and laminar flow. Note the parallel layers in laminar flow in direct contrast to the turbulent flow.

The effect of turbulence on the system can be difficult to characterize. Turbulence *can* be described by the Navier-Stokes equations, which relate velocity, temperature, pressure, and density of a moving fluid. They describe this relationship using conservation of mass and momentum in a system (NASA). However, without knowing all of the parameters in extensive detail and simulating them in accordance with the governing equations, we cannot predict the pressure and velocity at various locations under turbulence. However, Reynolds number can be a useful measure of turbulence. Reynolds is a dimensionless quantity defined by the equation:

$$Re = \frac{\rho \cdot V \cdot d}{\mu} \quad (6)$$

where  $\mu = 1.2 \times 10^{-5} \frac{kg}{m \cdot s}$  is the dynamic viscosity of air,  $\rho = 1.26 \frac{kg}{m^3}$  is the density of air, d is the diameter of the pipe and V is the velocity of the fluid. A Reynolds number of less than approximately 2300 indicates laminar flow, while a number higher than this indicates turbulent flow (Warhaft, 1997). We can approximate d with the diagonal length of the non-constricted section of our device. This turns out to be .032 m. Further, we can calculate V using the relation

$$V = \frac{Q}{A} \quad (7)$$

where Q is the volumetric flow rate and A is the cross-sectional area of our tube. Using the endpoints of our range of interest (.5 L/s to 1 L/s), we calculate a Reynolds number between 3400 and 6700. Thus, the flow through our device is definitively turbulent.

However, the ability of our code to produce a flow rate from pressure differences relies on the assumption of laminar flow. In order to create conditions closer to laminar flow, we designed an inlet diffuser with a series of parallel, vertical fins running along the axis of flow. In order to test the efficacy of this design and our turbulence hypothesis, we collected a series of

data points with the diffuser on the input of the tube and another series with the diffuser on the output of the tube. The results are shown in Figures 12A and 12B.

It can be seen that placing this diffuser on the input of the tube generally increased the difference between the measured and expected flow rates. More analysis needs to be done to confirm whether this is due to changes in turbulent flow, however, it is clear that, with our experimental setup, the diffuser on the input pushes the measured flow rate further from the expected flow rate.

Additionally, we investigated the effects that leakage has on our measurements. Leakage describes gasses exiting the tube anywhere other than the output port. In the intended setting, the tube should be entirely airtight. However, understanding the effect of leakage on the tube can help with further studies such as detecting leakage in the tube. One of the clearest differences between the tubes with and without leakage is that the measured pressure differences on the unsealed tube between the input and constriction sensors are about 55% of what they would be for the tube without leakage. This can be seen from the linear fit of the sealed tube with a slope of about 50.64, and the unsealed tube has a slope of about 28.03.

Thus, in our calculations of the flow rate we opted to use the pressure difference between the input sensor and the constriction sensor as the input sensor was much less affected by any leakage. As only one difference is required to calculate the flow rate, a third DPS310 sensor on the output side of the device is likely redundant. Furthermore, we found that the correction for atmospheric pressure drift using the ambient pressure sensor was negligible and therefore likely unnecessary as well. The removal of these two sensors from the system would further simplify the device and reduce its cost.

## Calibration Discussion

After having tested the effect of various geometries on the performance of the tube, it became crucial to develop a technique to calibrate the tube. Using the derived equations, the measured pressure difference between the input and middle sensors should vary linearly with the square of the flow rate. In order to demonstrate the procedure used to calibrate the tubes, we will consider the data from the tube with an inlet diffuser and the standard-length constriction. The set of average pressure differences was plotted against the square of the input flow rate used to produce those differences. A linear fit was performed returning  $y = 57.1 * x + 5.00$ . These values are very close to the expected slope of 58.08 and intercept of zero. The associated R-square value is 0.9996, showing a very strong linear fit. In general, for flow rates in the range of 0.5 to 1.5, the linear fit is an excellent approximation for the measured response. However, for smaller values, the actual data points sharply trail away from the line towards zero. One potential interpretation of this trend is that the boundary condition imposed by the tube leads to a certain degree of resistance to the flow that cannot be accounted for at a certain flow rate. As that cut-off flow rate is approached, the measured pressure differences quickly become smaller and smaller. This concept of a cut-off flow rate is supported by the intercept of the linear fit. We can assume the pressure drop between any two locations inside of the tube can have a contribution from the Bernoulli effect and a contribution from the frictional resistance to airflow. The Darcy-Weisbach equation states that the pressure loss between two points in a pipe is directly proportional to the length between those points and the square of the velocity. However, we have shown that the pressure measurements deviated more from the expected values for lower velocities, which contradicts the equation. It is apparent that there must be additional factors aside from straight pipe friction. These deviations may occur from resistance to flow in the constriction. Future

calibrations of the tube should incorporate the losses due to both straight pipe friction and other resistances to potentially account for the divergence from the linear fit at low flow rates.

## Conclusions

Access to life-saving ventilation can become extremely difficult in developing countries and in developed countries during a pandemic. A quick solution to ease some of the strain on the healthcare infrastructure is to share ventilators among patients. In order to ensure that this is done as safely and effectively as possible, we have presented a low-cost, high-resolution flow meter that can be implemented in line with the ventilator. The flow sensor can be reliably constructed from plastic, printed circuit boards, and commercially available electronic components. The code and microcontroller are easy to access. We were able to show that the pressure differences can be fitted to a line with a high r-square value, showing their potential to measure flow rate. Future investigations must account for the divergence from the linear fit for small pressure differences. We investigated various parameters such as tube length and the inclusion of a diffuser. With the limited data we have, we were unable to definitively determine the effects of these on the performance of the tube. However, it is evident that there is potential for the tube to be implemented as an oxygen flow rate monitor.

## References

- Alex, C.G. (n.d.) *Mechanical Ventilation*. Loyola University Chicago LUMEN.  
[http://www.meddean.luc.edu/lumen/meded/MEDICINE/PULMONAR/lecture/vent\\_f.htm](http://www.meddean.luc.edu/lumen/meded/MEDICINE/PULMONAR/lecture/vent_f.htm)
- Anderson, J. D. (2007). *Fundamentals of Aerodynamics*. McGraw-Hill.
- Auld, S.C., Caridi-Scheible, M., Blum, J.M., Robichaux, C., Kraft, C., Jacob, J.T., Jabaley, C.S., Carpenter, D., Kaplow, R., Hernandez-Romieu, A.C., Adelman, M.W., Martin, G.S., Coopersmith, C.M., & Murphy, D.J. (2020, April 26) *ICU and ventilator mortality among critically ill adults with COVID-19*. National Institutes of Health.  
<https://www.ncbi.nlm.nih.gov/pmc/articles/PMC7276026/>
- American Thoracic Society. (2020, April) *Mechanical Ventilation*.  
<https://www.thoracic.org/patients/patient-resources/resources/mechanical-ventilation.pdf>
- Corvallis Forestry Research Community. (2006) *Darcy Friction Factor*.  
[http://www.fsl.orst.edu/geowater/FX3/help/8\\_Hydraulic\\_Reference/Darcy\\_Friction\\_Factor.htm](http://www.fsl.orst.edu/geowater/FX3/help/8_Hydraulic_Reference/Darcy_Friction_Factor.htm)
- Gollin, G. (2021, October 6) *Bernoulli flow sensors for monitoring oxygen delivery by a multi-patient respirator*. PHYS 398DLP.  
[https://courses.physics.illinois.edu/phys398dlp/fa2021/secure/group2\\_circuit.pdf](https://courses.physics.illinois.edu/phys398dlp/fa2021/secure/group2_circuit.pdf)
- Hurtado, C. (2018, May 3) *Ventilator Stockpiling and Availability in the US and Internationally*. Clade X.  
[https://www.centerforhealthsecurity.org/our-work/events/2018\\_clade\\_x\\_exercise/pdfs/Clade-X-ventilator-availability-fact-sheet.pdf](https://www.centerforhealthsecurity.org/our-work/events/2018_clade_x_exercise/pdfs/Clade-X-ventilator-availability-fact-sheet.pdf)

Infineon Technologies AG. (2020, October 15) *DPS310*.

[https://www.infineon.com/dgdl/Infineon-DPS310-DataSheet-v01\\_01-EN.pdf?fileId=546d462576f34750157750826c42242](https://www.infineon.com/dgdl/Infineon-DPS310-DataSheet-v01_01-EN.pdf?fileId=546d462576f34750157750826c42242)

Maclean, R. & Marks, S. (2020, April 18) *10 African Countries Have No Ventilators. That's Only Part of the Problem.* The New York Times.

<https://www.nytimes.com/2020/04/18/world/africa/africa-coronavirus-ventilators.html>

NASA. (n.d. a) *Bernoulli's Principle*.

[https://www.nasa.gov/sites/default/files/atoms/files/bernoulli\\_principle\\_k-4.pdf](https://www.nasa.gov/sites/default/files/atoms/files/bernoulli_principle_k-4.pdf)

NASA. (n.d. b) *Navier-Stokes Equations*.

<https://www.grc.nasa.gov/www/k-12/airplane/nseqs.html>

Nuclear Power. (n.d.) *Turbulent Flow*.

<https://www.nuclear-power.com/nuclear-engineering/fluid-dynamics/turbulent-flow/>

Rosenthal, B.M. (2020, March 27). '*The Other Option Is Death*': New York Starts Sharing of *Ventilators*. The New York Times.

<https://www.nytimes.com/2020/03/26/health/coronavirus-ventilator-sharing.html>

Stanmech Technologies. (2019, February 21) *Understanding the Difference Between Flow, Velocity, and Pressure*. <https://www.stanmech.com/articles/flow-velocity-and-pressure>

U.S. Food and Drug Administration. (2021, February 9) *Using Ventilator Splitters During the COVID-19 Pandemic - Letter to Health Care Providers*.

<https://www.fda.gov/medical-devices/letters-health-care-providers/using-ventilator-splitters-during-covid-19-pandemic-letter-health-care-providers>

Warhaft, Z. (1997) *Transition and Turbulence*. Princeton.

[https://www.princeton.edu/~asmits/Bicycle\\_web/transition.html](https://www.princeton.edu/~asmits/Bicycle_web/transition.html)

Warner, M. A., & Patel, B. (2013). Chapter 48 - Mechanical ventilation. *Benumof and Hagberg's Airway Management*, 981–997. <https://doi.org/10.1016/b978-1-4377-2764-7.00048-8>